Adaptive Decentralized Droop Controller to Preserve Power Sharing Stability of Paralleled Inverters in Distributed Generation Microgrids

Yasser Abdel-Rady Ibrahim Mohamed and Ehab F. El-Saadany, *Senior Member, IEEE*

***Abstract*—This paper addresses the low-frequency relative stability problem in paralleled inverter-based distributed generation (DG) units in microgrids. In the sense of the small-signal dynamics of a microgrid, it can be shown that as the demanded power of each inverter changes, the low-frequency modes of the power sharing dynamics drift to new locations and the relative stability is remarkably affected, and eventually, instability can be yielded. To preserve the power sharing stability, an adaptive decentralized droop controller of paralleled inverter-based DG units is presented in this paper. The proposed power sharing strategy is based on the static droop characteristics combined with an adaptive transient droop function. Unlike conventional droop controllers, which yield 1-DOF tunable controller, the proposed droop controller yields 2-DOF tunable controller. Subsequently, the dynamic performance of the power sharing mechanism can be adjusted, without affecting the static droop gain, to damp the oscillatory modes of the power sharing controller. To account for the power modes immigration at different loading conditions, the transient droop gains are adaptively scheduled via small-signal analysis of the power sharing mechanism along the loading trajectory of each DG unit to yield the desired transient and steady-state response. The gain adaptation scheme utilizes the filtered active and reactive powers as indices; therefore, a stable and smooth power injection performance can be obtained at different loading conditions. The adaptive nature of the proposed controller ensures active damping of power oscillations at different operating conditions, and yields a stable and robust performance of the paralleled inverter system.**

***Index Terms*—Adaptive control, decentralized control, distributed generation (DG), microgrid, parallel operation, power sharing stability.**

I. Introduction

DRIVEN by economical, technical, and environmental reasons, the energy sector is moving into an era where large portions of increases in electrical energy demand will be met through widespread installation of distributed resources, or what is known as distributed generation (DG) [1]. The use of DG increases the service reliability and reduces the need for future generation expansion or grid reinforcement. Moreover, it extends up the possibility of making the DG responsible for local power quality, voltage regulation, power factor correction, etc., in a way that is not possible with conventional centralized generators [2]. Unlike large generators, which are almost exclusively 50/60-Hz synchronous machines, DG units include variable frequency (variable speed) sources (such as wind energy sources), high-frequency (high-speed) sources (such as microturbines), and direct energy conversion sources producing dc voltages or currents (such as fuel cells and photovoltaic sources). The majority of distributed resources are interfaced to the utility grid/loads via dc–ac inverter systems [3], [4]. There are several operating regimes possible for DG. Among them is the microgrid [5], [6], in which a cluster of DG units serviced by a distribution system is formed to maintain the reliability of critical loads, mainly when the utility supply is not available. However, a reliable and robust operation of a microgrid centers on an efficient control scheme of microgrid generators.

The basic control objective in a microgrid is to achieve accurate power sharing while maintaining close regulation of the microgrid voltage magnitude and frequency. Centralized control of a microgrid, based on a communication infrastructure, is investigated in [7]. However, in microgrids in remote areas with long connection distance between inverters, it is impractical and costly to distribute the dynamic sharing signals, which are characterized by their high bandwidth. Further, reliability issues of the centralized control approach might counteract the positive reliability boosts gained by implementing DG microgrids. To overcome these limitations, decentralized controllers are reported. A signal injection technique is used as a power sharing mechanism in paralleled inverters system [8]. However, the complexity of signal injection and the robustness of measuring output power variations caused by the injected signal make this scheme far from being practical. Droop controllers, which emulate the droop characteristic of synchronous generators, are proposed as power sharing controllers of microgrid generators [9]–[12]. A static droop compensator is utilized for power sharing in [9] and [10]. An enhanced droop control featuring a transient droop performance is proposed in [11]. To improve the active and reactive power decoupling performance, improved droop controllers with virtual output impedance are reported [11], [12]. To account for nonlinear loads, harmonic-based droop controllers are investigated [13], [14]. In fact, the power sharing controller dictates the low-frequency dynamics of the inverter due to the time-scale separation between the power, voltage, and current dynamics. However, existing droop controllers are synthesized in the sense of the small-signal model of the power transfer mechanisms; this can yield acceptable results for small load variation. In a typical microgrid system, the concept of "base-load" might not be applied; accordingly, large load variations are expected. In the sense of the microgrid dynamics,

Manuscript received January 20, 2008; revised May 18, 2008. Current version published December 9, 2008. Recommended for publication by Associate Editor M. Ponce-Silva.

The authors are with the Department of Electrical and Computer Engineering, University of Waterloo, Waterloo, ON N2L 3G1, Canada (e-mail: yasser_rady@ieee.org).

Digital Object Identifier 10.1109/TPEL.2008.2005100

it can be shown that as the demanded power of each inverter changes, the low-frequency modes of the power sharing dynamics drift to new locations yielding different dynamic performance. In particular, at higher power demands, the damping active/reactive powers required to stabilize the frequency/voltage are limited. In this case, the dominant modes of the power sharing dynamics move toward unstable region, making the system more oscillatory, and eventually, instability can be yielded. The low damping feature of the oscillatory power modes yields low-frequency oscillations in the fundamental-voltage frequency, and low-frequency oscillations will be imposed on the injected currents, which might excite unstable dynamics. In addition, the low damping of the power controller modes generates dynamic coupling among the active and reactive power components; yielding poor sharing and might force large transient startup and circulating currents. Due to the limited thermal time constant of an inverter-based DG unit, the overload capability of these generators is limited; 1.2–1.5 per unit (p.u.) for less than half a cycle [15]. Accordingly, a microgrid collapse scenario is very likely to take place due to the poor damping performance of the power sharing mechanism.

To override the aforementioned problems, a decentralized control of microgrid inverters using adaptive power sharing controller is presented in this paper. The power sharing strategy is based on the static droop characteristics combined with an adaptive transient droop function. Unlike conventional droop controllers, which yield 1-DOF tunable controller, the proposed droop controller yields 2-DOF tunable controller. Subsequently, the dynamic performance of the power sharing mechanism can be adjusted, without affecting the static droop gain, to damp the oscillatory modes of the power sharing controller. To account for the power modes immigration at different loading conditions, the transient droop gains are scheduled via small-signal analysis of the power sharing mechanism along the operation trajectory of each DG unit to yield the desired transient and steady-state response. The gain adaptation scheme utilizes the filtered active and reactive powers as indices; therefore, a smooth power injection performance can be obtained. The adaptive nature of the proposed controller ensures active damping of power oscillations at different operating conditions and yields a robust performance of the paralleled inverter system.

The remainder of this paper is organized as follows. In Section II, modeling of a microgrid-connected inverter-based DG unit is presented. In Section III, the power sharing dynamic performance in a microgrid with conventional droop controller is analyzed. In Section IV, the proposed power sharing controller is presented. Evaluation results are provided to demonstrate the effectiveness of the proposed control scheme in Section VI. Conclusions are drawn in Section VII.

II. Modeling of a Microgrid-Connected Voltage-Sourced Inverter (VSI)

Fig. 1 shows a microgrid system made of a cluster of inverter-based DG units empowered by microsources, such as fuel cells, microturbines, dc storage, etc. A dc/ac VSI is commonly used as an interfacing module. Fig. 2 shows a block diagram of a

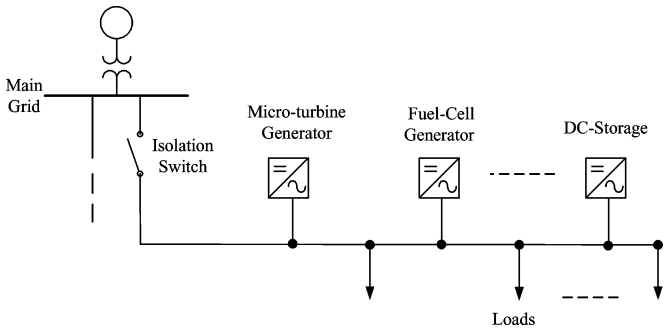

Fig. 1. Microgrid system.

microgrid-connected VSI. A three-leg VSI with an *LC* filter with a coupling inductor form the power circuit, whereas three control loops form the control structure. Specifically, a power sharing controller is used to generate the magnitude and frequency of the fundamental output voltage of the inverter according to the droop characteristic, by emulating the operation of a conventional synchronous generator; a voltage controller is used to synthesize the reference filter–inductor current vector; and a current controller is adopted to generate the command voltage vector to be synthesized by a pulse-width-modulation (PWM) module. Both the voltage and current control loops should provide enough damping for the output *LCL* filter composed of the *LC* filter combined with the coupling inductor. The coupling inductor shapes the output impedance of the inverter so that the active–reactive power coupling is minimized.

In Park's d–q frame that rotates synchronously with the inverter output voltage angular speed $\omega_{\rm o}$, the current and voltage dynamics can be reasonably represented by the following equations:

$$\frac{di_d}{dt} = \frac{-R_f}{L_f} i_d + \omega_{\rm o} i_q + \frac{1}{L_f}\left(v_d - v_{\rm od}\right) \tag{1}$$

$$\frac{di_q}{dt} = \frac{-R_f}{L_f} i_q - \omega_{\rm o} i_d + \frac{1}{L_f}\left(v_q - v_{\rm oq}\right) \tag{2}$$

$$\frac{dv_{\rm od}}{dt} = \omega_{\rm o} v_{\rm oq} + \frac{1}{C_f}\left(i_d - i_{\rm od}\right) \tag{3}$$

$$\frac{dv_{\rm oq}}{dt} = -\omega_{\rm o} v_{\rm od} + \frac{1}{C_f}\left(i_q - i_{\rm oq}\right) \tag{4}$$

$$\frac{di_{\rm od}}{dt} = \frac{-R_c}{L_c} i_{\rm od} + \omega_{\rm o} i_{\rm oq} + \frac{1}{L_c}\left(v_{\rm od} - v_{sd}\right) \tag{5}$$

$$\frac{di_{\rm oq}}{dt} = \frac{-R_c}{L_c} i_{\rm oq} - \omega_{\rm o} i_{\rm od} + \frac{1}{L_c}\left(v_{\rm oq} - v_{sq}\right) \tag{6}$$

where v_d, v_q, i_d, and i_q are the d- and q-axis inverter's voltages and currents; $v_{\rm od}$, $v_{\rm oq}$, $i_{\rm od}$, and $i_{\rm oq}$ are the d- and q-axis output voltages and currents; v_{sd} and v_{sq} are the d- and q-axis bus voltages, R_f, L_f, and C_f are the per-phase resistance, inductance, and capacitance of the *LC* filter, respectively; and R_c and L_c are the per-phase resistance and inductance of the coupling inductor, respectively.

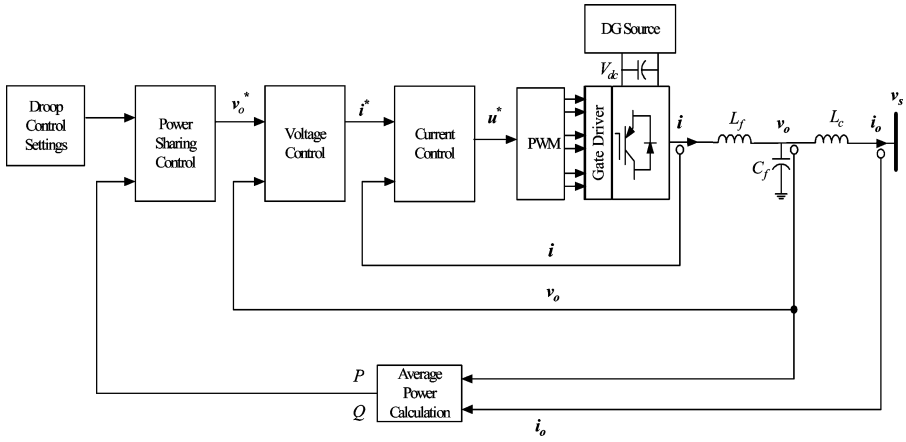

Fig. 2. Power circuit and control structure of a microgrid-connected VSI.

Using the two-axis theory, the injected instantaneous active and reactive power components, p and q, are given by

$$p = v_{\mathrm{od}} i_{od} + v_{\mathrm{oq}} i_{oq} \tag{7}$$

$$q = v_{\mathrm{od}} i_{\mathrm{oq}} - v_{\mathrm{oq}} i_{\mathrm{od}}. \tag{8}$$

To allow sufficient time-scale separation between the power and current control loops and to achieve high power quality injection, the average active and reactive powers corresponding to the fundamental components are subjected to control action, and they are obtained by means of a low-pass filter as

$$P = \frac{\omega_c}{s + \omega_c} p \tag{9}$$

$$Q = \frac{\omega_c}{s + \omega_c} q \tag{10}$$

where ω_c is the filter cutoff frequency.

To realize a power sharing function, the conventional droop characteristics are usually used in paralleled inverter systems to introduce the following droops in the fundamental voltage frequency and magnitude of the output voltage:

$$\omega_o = \omega^* - mP \tag{11}$$

$$v_{\mathrm{od}}^* = V^* - nQ \tag{12}$$

where ω^* and V^* are the nominal frequency and voltage set points, respectively, and m and n are the static droop gains, and they can be calculated for a given range of frequency and voltage magnitude as follows:

$$m = \frac{\omega_{\max} - \omega_{\min}}{P_{\max}} \tag{13}$$

$$n = \frac{V_{od\max} - V_{od\min}}{Q_{\max}}. \tag{14}$$

The set points in (11) and (12) act as a virtual communication agent for different inverters for autonomous operation. Also, the d-component of the output voltage is used in (14); as per the voltage-oriented control, the reference of the output voltage magnitude is aligned with the d-axis of the inverter reference frame.

To provide close voltage regulation, inverter output voltage control is adopted. The controller employs standard proportional–integral (PI) regulators with decoupling and feedforward control loops to generate the reference current vector. The dynamics of the voltage controller can be given by

$$i_d^* = K_{pv}(v_{\mathrm{od}}^* - v_{\mathrm{od}}) + K_{iv} \int (v_{\mathrm{od}}^* - v_{\mathrm{od}})\, dt - \omega^* C_f v_{\mathrm{oq}} + H i_{\mathrm{od}} \tag{15}$$

$$i_q^* = K_{pv}(v_{\mathrm{oq}}^* - v_{\mathrm{oq}}) + K_{iv} \int (v_{\mathrm{oq}}^* - v_{\mathrm{oq}})\, dt + \omega^* C_f v_{\mathrm{od}} + H i_{\mathrm{oq}} \tag{16}$$

where K_{pv}, K_{iv} are the proportional and integral gains, respectively, C_f is the filter capacitance, and H is the feedforward gain.

A current controller is needed to shape the voltage across the filter inductor, so that minimum current error is yielded. A standard PI current regulator with decoupling and feedforward control loops is adopted for current regulation. The dynamics of the current controller can be given by

$$v_d^* = K_{pi}(i_d^* - i_d) + K_{ii} \int (i_d^* - i_d) dt - \omega^* L_f i_q + v_{\mathrm{od}} \tag{17}$$

$$v_q^* = K_{pi}(i_q^* - i_q) + K_{ii} \int (i_q^* - i_q) dt + \omega^* L_f i_d + v_{\mathrm{oq}} \tag{18}$$

where K_{pi}, K_{ii} are the proportional and integral gains, respectively.

It should be noted that more advanced current and voltage controls can be applied to the DG interface [16], [17]; however, standard PI-based voltage and current controls are applied in this study, where the main scope is the power sharing stability and control design.

Equations (1)–(18) describe the dynamic behavior of a single inverter unit with the conventional droop controller. Small-signal analysis can provide a useful tool to analyze the dynamic performance and to design the control system [10], [18]; the aforesaid equations can be linearized and the following

state-space model of a single inverter unit can be obtained:

$$\Delta \dot{\boldsymbol{x}}_{\mathrm{DG}} = \boldsymbol{A}_{\mathrm{DG}} \Delta \boldsymbol{x}_{\mathrm{DG}} + \boldsymbol{B}_{\mathrm{DG}} \Delta \boldsymbol{v}_s \tag{19}$$

where

$$\Delta \boldsymbol{x}_{\mathrm{DG}} = [\,\Delta\delta \;\Delta P \;\; \Delta Q \;\; \Delta C_V \;\; \Delta C_C \;\; \Delta i_{dq} \;\; \Delta v_{odq} \;\; \Delta i_{odq}\,]^T$$

in which, δ represents the angle between the inverter reference frame and a common reference frame; C_V and C_c are the states of the voltage and current controllers (the integrator states), respectively; $\boldsymbol{v}_s$ is the supply voltage at the point of common coupling (PCC) transferred to a common reference frame; and $\boldsymbol{A}_{\mathrm{DG}}$ and $\boldsymbol{B}_{\mathrm{DG}}$ are the state and input matrices, and they are given as shown at the bottom of this page.

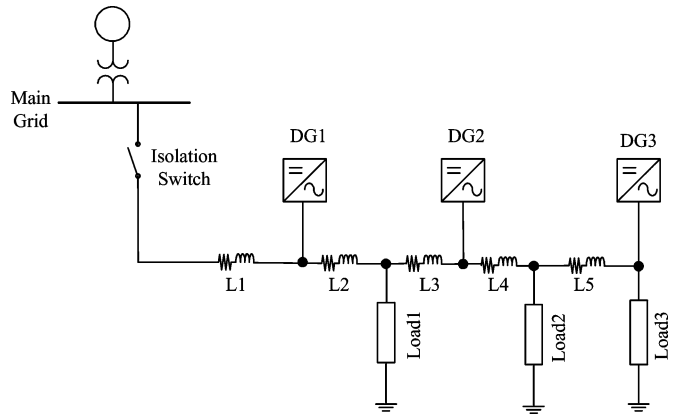

Fig. 3. Microgrid study system.

III. Power Sharing Dynamic Performance in a Microgrid With Conventional Droop Controller

To study the dynamic behavior of the power sharing mechanism in a microgrid, the small-signal dynamic model of the microgrid is constructed. The overall model embeds individual small-signal models of different inverters combined with the small-signal models of the network impedances including the load dynamics. It is more accurate to represent the dynamic models of the network and loads by their equivalent differential equations. The conventional approach in power system stability analysis is to represent these subsystems by a static relation based on the circuit phasor equations [20]. However, in a microgrid system, where the grid size is limited, there is a room to embed these dynamics to evaluate all possible dynamic modes.

A test microgird system is depicted in Fig. 3. The test system parameters are given in the Appendix.

The overall linearized model of a microgrid system can be given in the standard from of

$$\Delta \dot{\boldsymbol{x}} = \boldsymbol{A} \Delta \boldsymbol{x} + \boldsymbol{B} \Delta \boldsymbol{u}. \tag{20}$$

For the system under study, the state vector of the microgrid in (20) includes the states of the three inverters and the line and load states (determined by the number of energy storage elements in the network).

Fig. 4 shows the complete modes of the microgird study system, obtained at the steady-state initial operating conditions (0.7 p.u. loading of the microgrid), which are evaluated by means of load flow analysis. Fig. 4 indicates that a wide band of dynamic modes can be observed in the microgrid system. The frequency-scale separation between different modes is expected due to the time-scale separation between different control loops. The low-frequency modes are dictated mainly by the power sharing controllers and the power filters, which are designed with low bandwidth (around 2–10 Hz). The medium-frequency modes are mainly dictated by the voltage control loops, which are designed with medium bandwidths (400–600 Hz). The high-frequency modes are dictated by the *LCL* filters and the current control loops, which should be designed with high resonance

$$\boldsymbol{A}_{\mathrm{DG}} = \begin{bmatrix}
0 & -m & 0 & 0 & 0 & 0 & 0 & 0 & 0 & 0 & 0 & 0 & 0 \\
0 & -\omega_c & 0 & 0 & 0 & 0 & 0 & 0 & 0 & \omega_c I_{od} & \omega_c I_{od} & \omega_c V_{od} & \omega_c V_{oq} \\
0 & 0 & -\omega_c & 0 & 0 & 0 & 0 & 0 & 0 & \omega_c I_{oq} & -\omega_c I_{od} & -\omega_c V_{oq} & \omega_c V_{od} \\
0 & 0 & -n & 0 & 0 & 0 & 0 & 0 & 0 & -1 & 0 & 0 & 0 \\
0 & 0 & 0 & 0 & 0 & 0 & 0 & 0 & 0 & 0 & -1 & 0 & 0 \\
0 & 0 & -nK_{pv} & K_{pi} & 0 & 0 & 0 & -1 & 0 & -K_{pv} & -\omega^* C_f & H & 0 \\
0 & 0 & 0 & 0 & K_{pi} & 0 & 0 & 0 & -1 & \omega^* C_f & -K_{pv} & 0 & H \\
0 & -mI_q & \frac{-nK_{pi}K_{pv}}{L_f} & \frac{K_{pi}}{L_f} & 0 & \frac{K_{ii}}{L_f} & 0 & \frac{-K_{pi}-R_f}{L_f} & \omega_{\mathrm{o}} - \omega^* & \frac{-1-K_{pi}K_{pv}}{L_f} & \frac{-\omega^* C_f K_{pi}}{L_f} & \frac{K_{pi}H}{L_f} & 0 \\
0 & mI_d & 0 & 0 & \frac{K_{pi}}{L_f} & 0 & \frac{K_{ii}}{L_f} & \omega_{\mathrm{o}} - \omega^* & \frac{-K_{pi}-R_f}{L_f} & \frac{\omega^* C_f K_{pi}}{L_f} & \frac{-1-K_{pi}K_{pv}}{L_f} & 0 & \frac{K_{pi}H}{L_f} \\
0 & -mV_{oq} & 0 & 0 & 0 & 0 & 0 & \frac{1}{C_f} & 0 & 0 & \omega_{\mathrm{o}} & \frac{-1}{C_f} & 0 \\
0 & mV_{od} & 0 & 0 & 0 & 0 & 0 & 0 & \frac{1}{C_f} & -\omega_{\mathrm{o}} & 0 & 0 & \frac{-1}{C_f} \\
\frac{1}{L_c}\begin{pmatrix} V_{sD}\sin\delta_{\mathrm{o}} \\ -V_{sQ}\cos\delta_{\mathrm{o}} \end{pmatrix} & -mI_{oq} & 0 & 0 & 0 & 0 & 0 & 0 & 0 & \frac{1}{L_c} & 0 & \frac{-R_c}{L_c} & \omega_{\mathrm{o}} \\
\frac{1}{L_c}\begin{pmatrix} V_{sD}\cos\delta_{\mathrm{o}} \\ +V_{sQ}\sin\delta_{\mathrm{o}} \end{pmatrix} & mI_{od} & 0 & 0 & 0 & 0 & 0 & 0 & 0 & 0 & \frac{1}{L_c} & -\omega_{\mathrm{o}} & \frac{-R_c}{L_c}
\end{bmatrix}$$

$$\boldsymbol{B}_{\mathrm{DG}} = \begin{bmatrix}
0 & 0 & 0 & 0 & 0 & 0 & 0 & 0 & 0 & 0 & 0 & \frac{-1}{L_c}\cos\delta_{\mathrm{o}} & \frac{-1}{L_c}\sin\delta_{\mathrm{o}} \\
0 & 0 & 0 & 0 & 0 & 0 & 0 & 0 & 0 & 0 & 0 & \frac{-1}{L_c}\sin\delta_{\mathrm{o}} & \frac{-1}{L_c}\cos\delta_{\mathrm{o}}
\end{bmatrix}^T$$

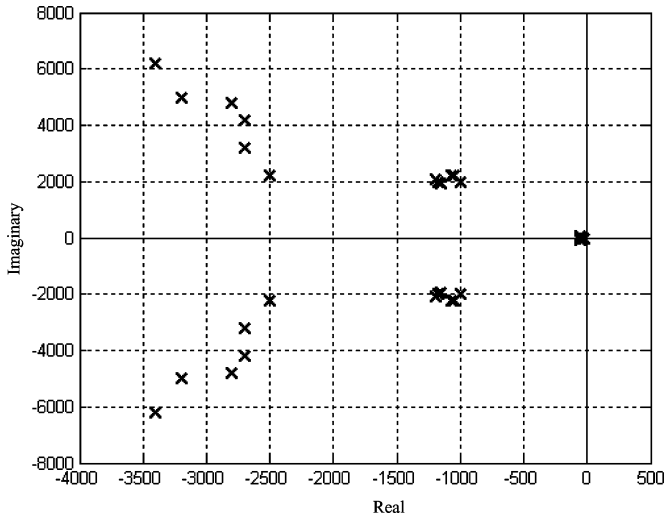

Fig. 4. Complete eigenvalues of microgrid study system (0.7 p.u. loading).

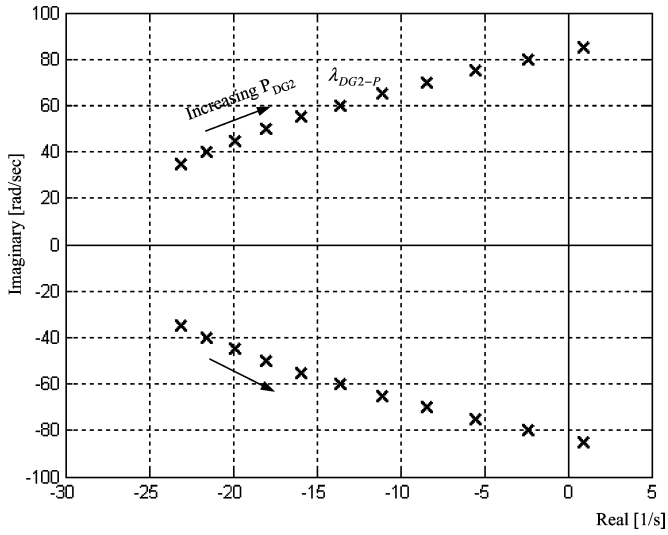

Fig. 5. Dominant low-frequency modes of DG2 with increasing output active power.

frequencies (in the range of 1.5 kHz). It should be noted that the aforementioned frequency/time separation is necessary and intentionally designed in a typical inverter system. For a given switching frequency, which is mainly dictated by the inverter's rating to constrain the switching losses, the maximum bandwidth of the inner current control loop is determined accordingly. On the other hand, the resonance frequency of the ac filter should be designed with enough margins from the first switching frequency to avoid any harmonic resonance at the switching frequency. At the same time, the resonance frequency should not be very low to avoid any low-order harmonic resonance due to grid voltage harmonics. In case of high-power inverters, the resonance frequency of the *LCL* filter should be lower to provide better filtering properties. Under these practical design and cost constraints, a typical current-controlled DG inverter can be designed with a current control loop bandwidth of about 1.0–1.5 kHz for medium- and high-power inverters. Since microgrid inverters should generate a regulated power, a voltage control loop is usually adopted to generate the reference current vector for the inner current loop. As a cascaded control system, the voltage control loop should be designed with a bandwidth that is at least three to five times slower than that of the inner current loop to preserve the stability and tracking resolution of the reference current command. The outermost control loop, which is the power control loop, should be designed with much lower bandwidth for two reasons. First, in case of grid- or microgrid-connected inverters, the average power control is adopted to ensure high power quality injection.[1] In this case, the outer power control loop should offer a relatively slowly changing reference voltage vector. Second, to extract the average power components from the measured *dq* instantaneous power components, low-pass filters with low cutoff frequencies should be designed. As a result, the outer average power control loop will roughly be designed with a bandwidth in the range of 2–10 Hz.

[1]On the contrary, instantaneous and direct power control techniques offer a relatively high bandwidth, and they are more suitable for active power conditioners and active rectifiers.

Therefore, the frequency separation is a salient feature that inherently exists in a well-designed inverter system. Therefore, even with different inverters, the frequency separation between different dynamic modes will inherently exist [10]. It should be noted that the power response time with the conventional droop controller might not be the same for different inverters within the microgrid. This is due to the setting of the droop gains according to the regulation requirements and the inverter ratings. In other words, the power ramping time of different inverter-based generators will not be the same. From the microgrid operation perspective, more robust control performance can be achieved when different units operate with close power response times that can also be controlled without affecting the regulation performance. This is one of the main objectives of the proposed microgrid control scheme.

Fig. 4 reveals that the power sharing states dictate the dominant dynamics of the microgrid system. Fig. 5 shows a trace of the dominant low-frequency mode of DG2, which can be evaluated using eigen-participation analysis, as the active output power of DG2 increases from 0.5 to 20 kW. It is clear in Fig. 5 that the damping of the dominant low-frequency mode is highly dependent on the operating condition. Fig. 5 indicates that the mode can be unstable by increasing the output power of the DG unit. Even with small changes around the operating point, the relative stability is remarkably affected; hence power oscillations are yielded.

The eigen-participation analysis confirms that the low-frequency modes are mainly dictated by the droop controller. Therefore, small-signal analysis of the power sharing droop controller can be a simplified tool to study the dominant dynamics of a microgrid system.

The conventional droop control law given in (11) controls the angular frequency of the inverter as a function of the real power output, under the conventional decoupling principle. The phase angle between the inverter reference frame and the voltage vector at the PCC (the power angle) is controlled accordingly to specify the amount of power transfer. The power transfer

equation that relates the average active output power to the power angle of the inverter can be given as follows:

$$P = \frac{V_{\rm o} V_s \sin(\delta_{\rm o} - \delta_s)}{X_c} \tag{21}$$

$$(\delta_{\rm o} - \delta_s) = \int (\omega_{\rm o} - \omega_s)\, dt \tag{22}$$

where $V_{\rm o}$ and V_s are the magnitudes of the inverter output voltage and the PCC voltage, respectively, $\delta_{\rm o}$ and δ_s are the phase angles of the inverter output voltage and the PCC voltage vector, respectively, and X_c is the reactance of the coupling inductor.

The small-signal model of (11), (21), and (22) can be constructed around an operating point ($\delta_{\rm o}^{\rm o}$,$\delta_s^{\rm o}$,$V_{\rm o}^{\rm o}$,$V_s^{\rm o}$) as follows:

$$\Delta P(s) = \frac{H_P}{s + mH_p}\Delta\omega^* - \frac{H_P}{s + mH_p}\Delta\omega_s \tag{23}$$

$$H_P = \frac{V_{\rm o}^{\rm o} V_s^{\rm o} \cos(\delta_{\rm o}^{\rm o} - \delta_s^{\rm o})}{X_c}. \tag{24}$$

From (11) and (23), it can be concluded that the droop gain m influences both the regulation and dynamic performance of the linearized active power transfer mechanism. The eigenvalue of (23) is given by

$$\lambda_{Po} = -mH_P. \tag{25}$$

If the droop gain is selected according to the regulation requirements, the eigenvalue in (25) will be directly determined by the operating condition. Accordingly, the damping of the dominant modes will be dependant on the output power, and the eigenvalue immigration will be significant, as shown in Fig. 5. It can be seen that the conventional droop controller lacks the ability of controlling the damping of the low-frequency power modes at different operating conditions without affecting the frequency regulation, which is a stiff requirement at steady-state operation.

The output voltage magnitude of the inverter is drooped as a function of the injected reactive power, as shown in (12). The relation between the voltage magnitude $V_{\rm o}$ and the corresponding output reactive power Q can be given by

$$Q = \frac{V_{\rm o}^2 - V_{\rm o} V_s \cos(\delta_{\rm o} - \delta_s)}{X_c}. \tag{26}$$

The small-signal model of (12) and (26) can be constructed around an operating point ($\delta_{\rm o}^{\rm o}$, $\delta_s^{\rm o}$, $V_{\rm o}^{\rm o}$, $V_s^{\rm o}$) as follows:

$$\Delta Q(s) = \frac{H_Q}{1 + nH_Q}\Delta V^*(s) + \frac{H_{Q2}}{1 + nH_Q}\Delta V_s(s) \tag{27}$$

$$H_Q = \frac{2V_{\rm o}^{\rm o} - V_s^{\rm o} \cos(\delta_{\rm o}^{\rm o} - \delta_s^{\rm o})}{X_c} \tag{28}$$

$$H_{Q2} = \frac{-V_{\rm o}^{\rm o} \cos(\delta_{\rm o}^{\rm o} - \delta_s^{\rm o})}{X_c}. \tag{29}$$

From (12) and (27), it can be concluded that the regulation performance is controllable by the droop gain n, whereas the dynamic performance of the linearized reactive power transfer mechanism is not controllable [20].

It should be noted that (25) shows that the eigenvalues of the active power sharing dynamics are real. However, due to the presence of the power filters (with a fixed pole in the s-domain, as given in (9) and (10), and the weak effect of coupling among power components, a third-order small-signal dynamics will characterize the power angle response. However, the damping is dominantly governed by (25) due to the dominant low damping nature of the sinusoidal P–δ dynamics, particularly at large power angle swings. To confirm this fact, let us consider the effects of the power filters and the P–Q coupling on the power angle dynamics. The coupled small-signal power transfer dynamics, around an operating point ($\delta_{\rm o}^{\rm o}$, $\delta_s^{\rm o}$, $V_{\rm o}^{\rm o}$, $V_s^{\rm o}$), can be constructed as follows:

$$\begin{bmatrix}\Delta P(s)\\ \Delta Q(s)\end{bmatrix} = \begin{bmatrix}\left(\frac{\partial P}{\partial(\delta_{\rm o}-\delta_s)}\right)_{\rm o} & \left(\frac{\partial P}{\partial V_{\rm o}}\right)_{\rm o}\\ \left(\frac{\partial Q}{\partial(\delta_{\rm o}-\delta_s)}\right)_{\rm o} & \left(\frac{\partial Q}{\partial V_{\rm o}}\right)_{\rm o}\end{bmatrix} \times \begin{bmatrix}\Delta(\delta_{\rm o}-\delta_s)(s)\\ \Delta V_{\rm o}(s)\end{bmatrix}. \tag{30}$$

Since the calculated power components are low-pass filtered to extract the average power components, hence the filter effect can be incorporated in (30) as follows:

$$\begin{bmatrix}\Delta P_{\rm av}(s)\\ \Delta Q_{\rm av}(s)\end{bmatrix} = \begin{bmatrix}\frac{\omega_c}{s+\omega_c} & 0\\ 0 & \frac{\omega_c}{s+\omega_c}\end{bmatrix}\begin{bmatrix}\left(\frac{\partial P}{\partial(\delta_{\rm o}-\delta_s)}\right)_{\rm o} & \left(\frac{\partial P}{\partial V_{\rm o}}\right)_{\rm o}\\ \left(\frac{\partial Q}{\partial(\delta_{\rm o}-\delta_s)}\right)_{\rm o} & \left(\frac{\partial Q}{\partial V_{\rm o}}\right)_{\rm o}\end{bmatrix} \times \begin{bmatrix}\Delta(\delta_{\rm o}-\delta_s)(s)\\ \Delta V_{\rm o}(s)\end{bmatrix}. \tag{31}$$

By adding the droop functions to (31), the following dynamics can be obtained:

$$\begin{bmatrix}\Delta\omega_{\rm o}(s)\\ \Delta V_{\rm o}(s)\end{bmatrix} = \begin{bmatrix}\Delta\omega^*(s)\\ \Delta V^*(s)\end{bmatrix} + \begin{bmatrix}\frac{-m\omega_c}{s+\omega_c} & 0\\ 0 & \frac{-n\omega_c}{s+\omega_c}\end{bmatrix} \times \begin{bmatrix}\left(\frac{\partial P}{\partial(\delta_{\rm o}-\delta_s)}\right)_{\rm o} & \left(\frac{\partial P}{\partial V_{\rm o}}\right)_{\rm o}\\ \left(\frac{\partial Q}{\partial(\delta_{\rm o}-\delta_s)}\right)_{\rm o} & \left(\frac{\partial Q}{\partial V_{\rm o}}\right)_{\rm o}\end{bmatrix} \times \begin{bmatrix}\frac{\Delta\omega_{\rm o}(s)-\Delta\omega_s(s)}{s}\\ \Delta V_{\rm o}(s)\end{bmatrix}. \tag{32}$$

Then, the dynamics of (32) is governed by the following characteristic equation:

$$s^3\Delta\omega_{\rm o}(s) + \alpha s^2\Delta\omega_{\rm o}(s) + \beta s\Delta\omega_{\rm o}(s) + \gamma\Delta\omega_{\rm o}(s) = 0 \tag{33}$$

where

$$\alpha = \omega_c\left(n\left(\frac{\partial Q}{\partial V_{\rm o}}\right)_{\rm o} + 2\right)$$

$$\beta = \omega_c\left(n\omega_c\left(\frac{\partial Q}{\partial V_{\rm o}}\right)_{\rm o} + m\left(\frac{\partial P}{\partial(\delta_{\rm o}-\delta_s)}\right)_{\rm o} + \omega_c\right)$$

$$\gamma = m\omega_c^2 \left(n \left(\frac{\partial P}{\partial (\delta_o - \delta_s)} \right)_o \left(\frac{\partial Q}{\partial V_o} \right)_o + \left(\frac{\partial P}{\partial (\delta_o - \delta_s)} \right)_o - n \left(\frac{\partial P}{\partial V_o} \right)_o \left(\frac{\partial Q}{\partial (\delta_o - \delta_s)} \right)_o \right).$$

Further, the sensitivity functions can be obtained as follows:

$$\left(\frac{\partial P}{\partial (\delta_o - \delta_s)} \right)_o = \frac{V_o^o V_s^o X_c \cos(\delta_o^o - \delta_s^o) + V_o^o V_s^o R_c \sin(\delta_o^o - \delta_s^o)}{R_c^2 + X_c^2} \quad (34)$$

$$\left(\frac{\partial P}{\partial V_o} \right)_o = \frac{V_s^o X_c \sin(\delta_o^o - \delta_s^o) - V_s^o R_c \cos(\delta_o^o - \delta_s^o) + 2V_o^o R_c}{R_c^2 + X_c^2} \quad (35)$$

$$\left(\frac{\partial Q}{\partial V_o} \right)_o = \frac{2V_o^o X_c - V_s^o X_c \cos(\delta_o^o - \delta_s^o) - V_s^o R_c \sin(\delta_o^o - \delta_s^o)}{R_c^2 + X_c^2} \quad (36)$$

$$\left(\frac{\partial Q}{\partial (\delta_o - \delta_s)} \right)_o = \frac{V_o^o V_s^o X_c \sin(\delta_o^o - \delta_s^o) - V_o^o V_s^o R_c \cos(\delta_o^o - \delta_s^o)}{R_c^2 + X_c^2}. \quad (37)$$

Using (33), the damping of the dominant eigenvalues can be traced along the whole loading trajectory. The obtained damping characteristics can be compared to those obtained by using (25). Note that the eigenvalue in (25) exactly describes the small-signal dynamics of $\Delta\omega_o(s)$ when it is derived from (23).

Fig. 6 depicts the damping of the dominant low-frequency mode as the active output power of DG2 increases from 0.5 to 20 kW by using (25) and (33). The close matching between both results confirms that a microgrid system can be stabilized by means of an active damping feature in the power sharing controller of each DG unit.

IV. Proposed Power Sharing Scheme

To overcome the aforementioned difficulties, a newly designed power sharing scheme is proposed. The power sharing controller adopts a modified droop function with controllable-gain transient droop characteristics. This configuration leads to a 2-DOF tunable controller, where the droop gain is selected to determine the frequency/voltage regulation performance and the transient gains can be adaptively tuned to damp the oscillatory modes at different operating conditions.

To provide means of adaptive active damping of the low-frequency power sharing modes and to increase the controllability of the reactive power sharing-controller, the following droop functions are proposed:

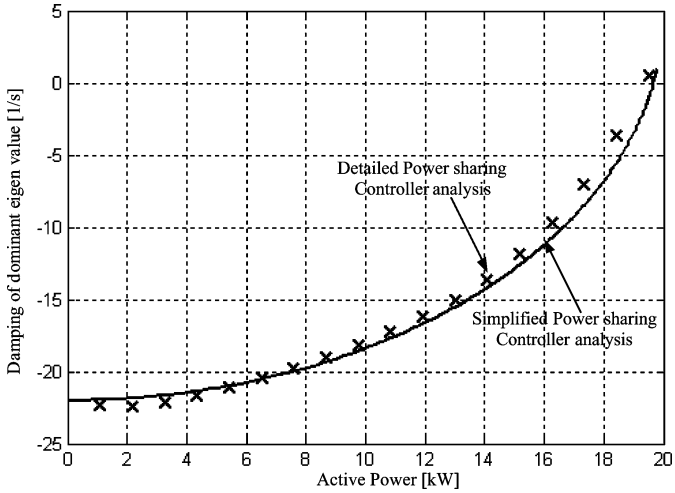

Fig. 6. Damping of the dominant low-frequency mode of DG2 with increase in output active power: Detailed power-sharing controller and simplified power sharing controller small signal analysis.

$$\omega_o = \omega^* - mP - \hat{m}_d \frac{dP}{dt} \quad (38)$$

$$v_{od}^* = V^* - nQ - \hat{n}_d \frac{dQ}{dt} \quad (39)$$

where $\hat{m}_d$ and $\hat{n}_d$ are adaptive transient droop gains.

The proposed droop functions employ additional derivative terms with adaptive gain. With this configuration, the power angle dynamics will be controlled in (38) with an equivalent PI control dynamics. Furthermore, the adaptation of the transient droop gain shapes the dynamic performance of the equivalent control dynamics in a manner that preserves the power sharing dynamic stability. The simplicity of the PI structure enables a simple first-order equivalent dynamics, where the adaptation mechanism can be derived as a pole placement problem. Similar observations can be extended to the proposed voltage droop function reported in (39). Accordingly, the aforesaid droop functions have been specifically selected. In what follows, a small-signal analysis will be presented to prove the salient features of the proposed controller in achieving robust power sharing performance with simple structure and easily derived adaptation gains.

The small-signal model of (21), (22), and (38) can be constructed around an operating point (δ_o^o, δ_s^o, V_o^o, V_s^o) as follows:

$$\Delta P(s) = \frac{H_P}{(1 + \hat{m}_d H_P)\, s + mH_P} \Delta\omega^* - \frac{H_P}{(1 + \hat{m}_d H_P)\, s + mH_P} \Delta\omega_s. \quad (40)$$

From (38) and (40), it can be seen that the regulation performance is decoupled from the dynamic performance of the linearized active power transfer mechanism. The eigenvalue of

(40) is

$$\lambda_P = \frac{-mH_P}{1+\hat{m}_d H_P}. \tag{41}$$

Therefore, the desired dynamic performance can be achieved by varying $\hat{m}_d$ without affecting the steady-state regulation performance set by m.

Similarly, the small-signal model of (26) and (39) can be constructed around an operating point (δ_o^o, δ_s^o, V_o^o, V_s^o) as follows:

$$\Delta Q(s) = \frac{H_Q}{\hat{n}_d H_Q s + (1+nH_Q)}\Delta V^*(s) + \frac{H_{Q2}}{\hat{n}_d H_Q s + (1+nH_Q)}\Delta V_s(s). \tag{42}$$

The eigenvalue of (42) is

$$\lambda_Q = \frac{-(1+nH_Q)}{\hat{n}_d H_Q} \tag{43}$$

which implies that the dynamic performance of the reactive power sharing controller can be adjusted by $\hat{n}_d$ without compromising the voltage regulation performance dictated by *n*.

Using (32), the adaptive gain $\hat{m}_d$ can be simply scheduled by means of the pole placement technique, mainly to adjust the damping of the active power sharing controller along the active power loading trajectory.

Using (41) and (43), the adaptive gains $\hat{m}_d$ and $\hat{n}_d$ can be simply scheduled by means of the pole placement technique, mainly to adjust the damping of the active and reactive power sharing controllers along the loading trajectory.

Fig. 7(a) shows a trace of $\hat{m}_d$ as a function of the output active power of DG2 to fix the damping of the active power sharing dynamics at $-50\ \mathrm{s}^{-1}$. It can be shown that the gain increases at high power levels to impose the additional damping required to constrain the dynamic performance of the active power sharing controller. Similarly, the adaptive gain $\hat{n}_d$ can be scheduled along the reactive power loading trajectory. Fig. 7(b) shows the gain schedule of $\hat{n}_d$ for DG2. The gain schedules of $\hat{m}_d$ and $\hat{n}_d$ utilize the static droop gains, which are fixed for each inverter unit, the preset eigenvalues, which are design parameters, and the coupling reactance X_c. The robustness against the uncertainty in X_c (90% X_{co} to 110% X_{co}, where the subscript "o" denotes the nominal value) is investigated, as shown in Fig. 7. It can be noticed that both the gain schedules show small sensitivity to the uncertainty in X_c. Accordingly, even with considerable variations in X_c, the damping of the power sharing modes will drift slightly from the preset values used to generate the gain schedules.

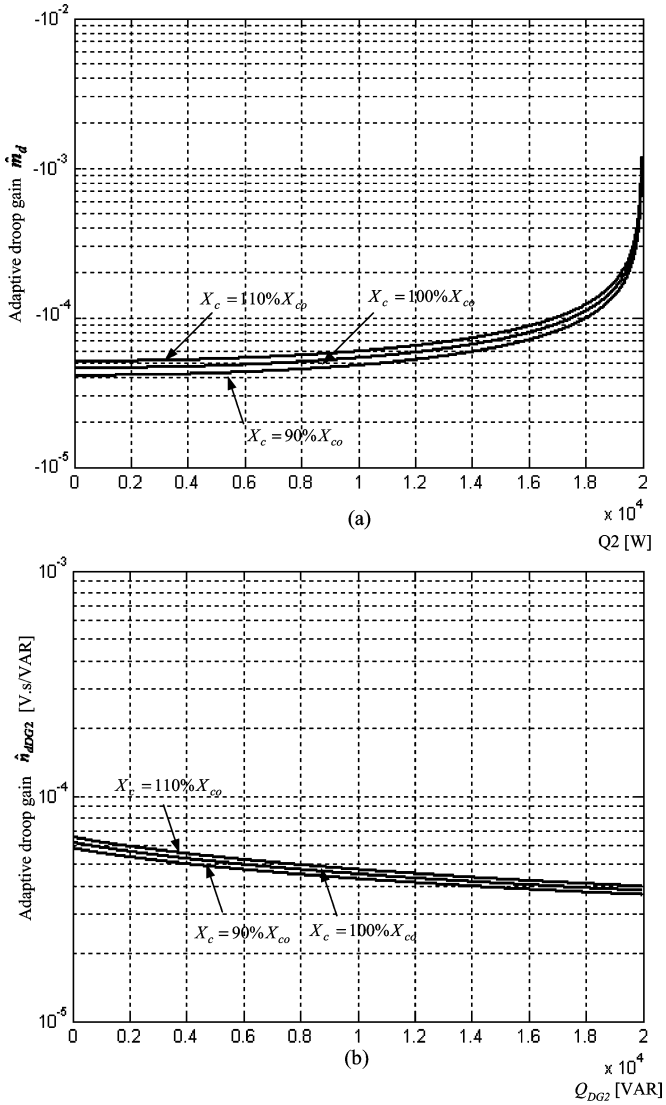

Fig. 7. Gain schedules of DG2. (a) $\hat{m}_d$. (b) $\hat{n}_d$.

V. Evaluation Results

To evaluate the performance of the proposed control scheme, the microgrid study system--depicted in Fig. 3 has been used. The system parameters are given in the Appendix. Each inverter unit employs the power circuit and control structure, as depicted in Fig. 2. The real-time code of the proposed control scheme is generated by the Real-Time WorkShop, under Matlab/Simulink environment. The TMS320C30 digital signal processor has been chosen as an embedded platform for real-time digital simulation experiments. The execution time of the control interrupt routine is about 120 μs. Subsequently, a control period $T = 150$ μs is selected. With this setting, a safe CPU load coefficient of 86% and a switching frequency of 6.7 kHz have been obtained. Since the sharp insulated-gate bipolar transistor commutation spikes may impair the current acquisition process, a synchronous sampling technique with a symmetric SVM module is adopted. With this method, the sampling is performed at the beginning of each modulation cycle. The current and voltage control loops are designed to yield bandwidth characteristics of 1.5 kHz and 0.5 kHz, respectively.

To verify the feasibility of the proposed controller, different operating conditions have been considered. For the purpose of performance comparison, the proposed control scheme is compared to the conventional droop controller. Some selected results are presented as follows.

A step change of 8 kW/3 kVAR increase in Load2 is considered. Fig. 8 shows the active power sharing performance of

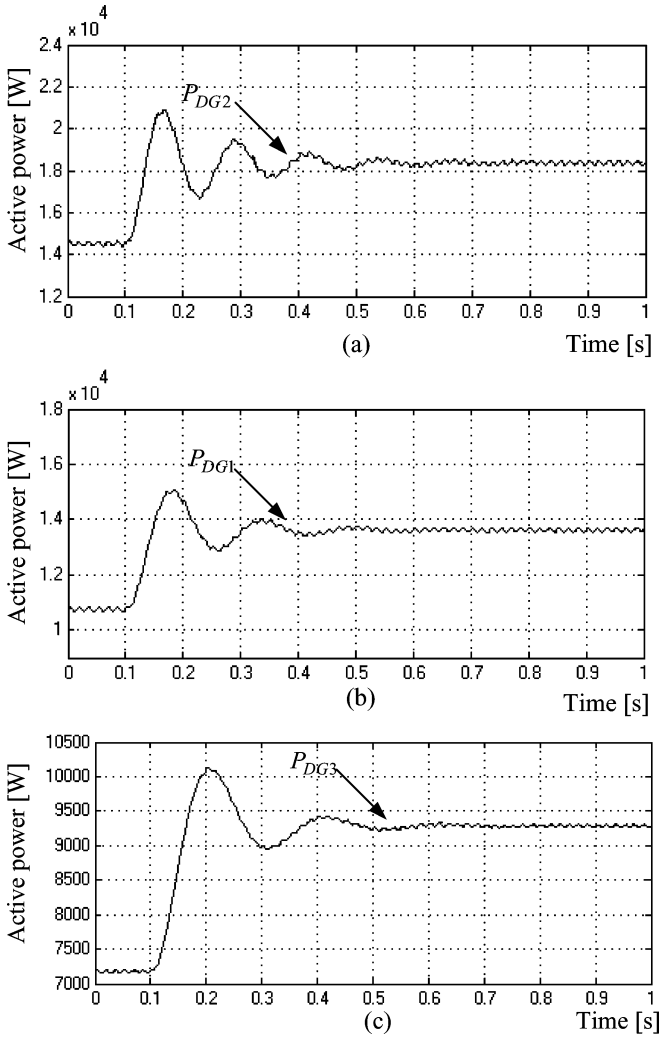

Fig. 8. Active power response of different DG units due to step change in Load2 with the conventional droop controller.

different DG units. The low damping of the dominant power sharing modes leads to a large transient response and oscillatory performance in the injected powers. For example, the power oscillations occur around 8 Hz with a damping around 7 s^{-1} for DG2; these results closely match the small-signal analysis results reported in Figs. 5 and 6. Since DG2 is closest to the load, the power performance of DG2 exhibits the largest transient response and it supplies most of the transient power due to the proximity to the load. For large power transients, the unit protection might be activated and the microgrid might not be able to maintain the load; hence, the overall system stability can be violated. Fig. 9 shows the reactive power sharing performance of different DG units. The total reactive power generation exceeds the load demand by 0.65 kVAR due to the reactive power requirement of the network lines and coupling filters of different DG units. The low-frequency modes can be traced in the injected reactive powers. However, they are less severe than those observed in the active power injections. This is due to the absence of the eigenvalue immigration problem in the conventional droop controller, as shown in (27).

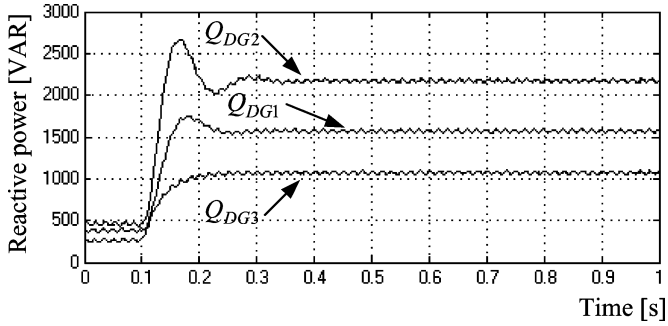

Fig. 9. Reactive power response of different DG units due to step change in Load2 with the conventional droop controller.

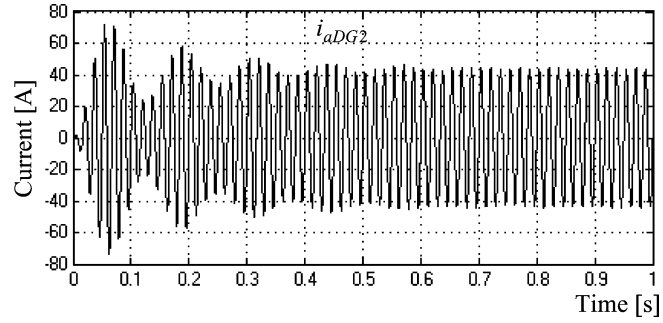

Fig. 10. Startup current of DG2 with the conventional droop controller.

Fig. 10 shows the startup phase-a current of DG2 with the conventional droop controller with 85% loading factor of DG2. It is obvious that the poorly damped power response leads to large transient currents that might overload the unit and activate the unit protection.

Under the same load disturbance, i.e., an 8 kW/3 kVAR increase in Load2, the proposed power sharing controller is tested. Fig. 11 (a), (c), and (e) shows the active power sharing performance of different DG units. It can be observed that the transient response is well damped and smooth power injection is yielded. Further, the load power is accurately shared according to the ratings of different generators. Fig. 11 (b), (d), and (f) shows the corresponding adaptive active droop gains of different DG units. Depending on the injected average active power, the $\hat{m}_d$ gain is adjusted to preserve a well-damped dynamic performance for each DG unit. Since the average power is used as an index for adaptation, smooth gain adaptation with high noise immunity is yielded for different DG units, as depicted in Fig. 11(b), (d), and (f).

Fig. 12 shows the reactive power sharing performance with the proposed controller. Fig. 12(a) shows the reactive power responses of different DG units. Damped reactive power sharing performance is yielded. Further, it can be noticed that the dynamic performance, in terms of the rise time, has been unified for different DG units. Fig. 12(b) shows the corresponding adaptive reactive droop gains of different DG units. Depending on the injected average active power, the $\hat{n}_d$ gain is adjusted to preserve a well-damped dynamic performance for each DG unit.

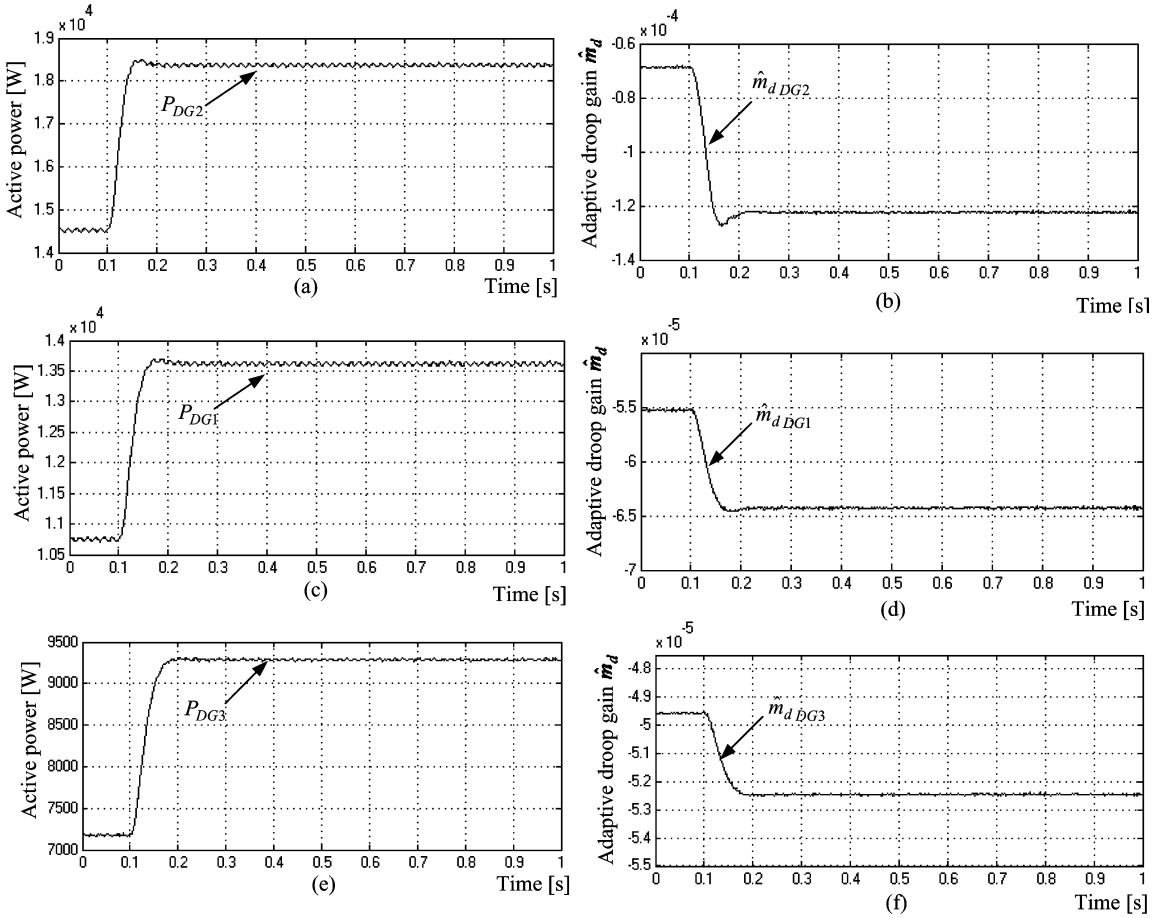

Fig. 11. Active power sharing performance with the proposed controller due to step change in Load2. (a), (c), and (e). Active power responses of different DG units. (b), (d), and (f). Corresponding adaptive active droop gains of different DG units.

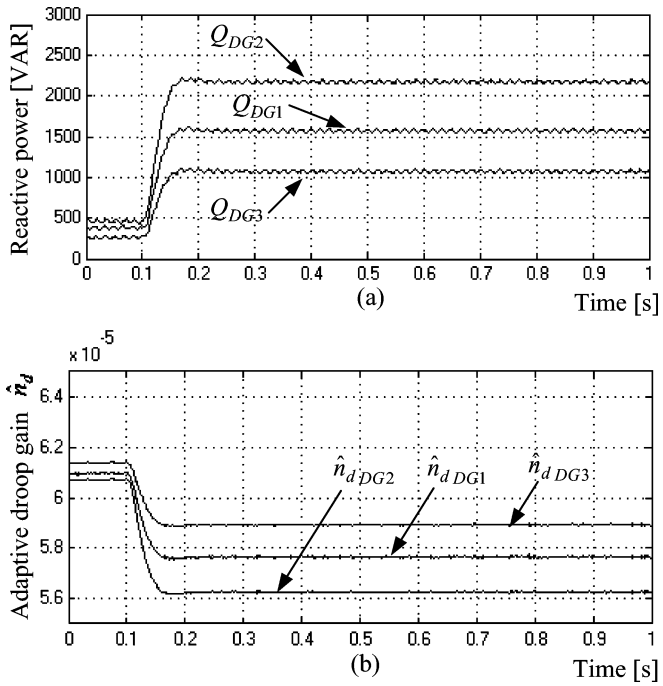

Fig. 12. Reactive power sharing performance with the proposed controller due to step change in Load2. (a) Reactive power responses of different DG units. (b) Corresponding adaptive reactive droop gains of different DG units.

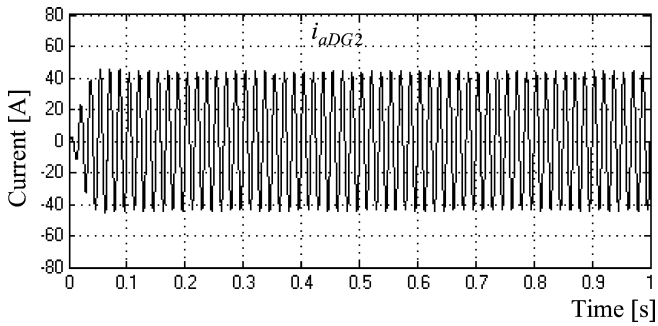

Fig. 13. Startup current of DG2 with the proposed droop controller.

Due to the damped transient response of the proposed controller, the transient startup currents can be significantly suppressed. This is obvious in Fig. 13, which depicts the startup phase-a current of DG2 using the proposed droop controller.

VI. Conclusion

An adaptive decentralized droop-based power sharing control scheme for paralleled inverters in DG microgrids has been presented in this paper. The proposed control structure preserves the dynamics and stability of each inverter unit at different loading conditions. The proposed power sharing strategy is based on the

static droop characteristics combined with an adaptive transient droop function. Unlike conventional droop controllers, which yield a 1-DOF tunable controller, the proposed droop controller yields a 2-DOF tunable controller. Subsequently, the dynamic performance of the power sharing mechanism can be adjusted, without affecting the static droop gain, to damp the oscillatory modes of the power sharing controller. To account for the power modes immigration at different loading conditions, the transient droop gains have been adaptively scheduled via small-signal analysis of the power sharing mechanism along the operation trajectory of each DG unit to yield the desired transient and steady-state response. Theoretical analysis and evaluation results reveal that the adaptive nature of the proposed controller ensures active damping of power oscillations at different operating conditions; subsequently, stable and robust power sharing performance has been obtained in the paralleled inverter system. As a result, the proposed scheme significantly contributes to preserving microgrid stability and reliability.

APPENDIX

The parameters of the studied system, shown in Fig. 3, are shown next

DG1: 15 kVA, 208 V (L–L), 60 Hz, $L_f = 1.5$ mH, $R_f = 0.15\,\Omega, C_f = 45\,\mu$F, $L_c = 0.53$ mH, $R_c = 0.05\,\Omega, m =$ 1.33e-4 rad/s/W, $n =$ 1.33e-3 V/VAR, $\omega_c = 30$ rad/s, $K_{pi} = 10$, $K_{ii} = 15300$, $K_{pv} = 0.045$, $K_{iv} = 400$, $H = 0.68$.

DG2: 20 kVA, 208 V (L–L), 60 Hz, $L_f = 1.5$ mH, $R_f = 0.15\ \Omega$, $C_f = 45\ \mu$F, $L_c = 0.53$ mH, $R_c = 0.05\ \Omega$, $m =$ 1e-4 rad/s/W, $n =$ 1e-3 V/VAR, $\omega_c = 30$ rad/s, $K_{pi} = 10$, $K_{ii} = 15300$, $K_{pv} = 0.045$, $K_{iv} = 400$, $H = 0.7$.

DG3: 10 kVA, 208 V (L–L), 60 Hz, $L_f = 1.5$ mH, $R_f = 0.15\ \Omega$, $C_f = 45\ \mu$F, $L_c = 0.53$ mH, $R_c = 0.05\ \Omega$, $m =$ 2e-4 rad/s/W, $n =$ 2e-3 V/VAR, $\omega_c = 30$ rad/s, $K_{pi} = 10$, $K_{ii} = 15300$, $K_{pv} = 0.045$, $K_{iv} = 400$, $H = 0.75$.

L1: $0.1 + 0.35j\ \Omega$, L2: $0.05 + 0.1j\ \Omega$, L3: $0.03 + 0.13j$, L4: $0.01 + 0.02j\ \Omega$, L5: 0.02 + $0.1j\ \Omega$.

REFERENCES

[1] "Special issue on distributed power generation," *IEEE Trans. Power Electron.*, vol. 19, no. 5, Sep. 2004.

[2] F. Blaabjerg, Z. Chen, and S. B. Kjaer, "Power electronics as efficient interface in dispersed power generation systems," *IEEE Trans. Power Electron.*, vol. 19, no. 5, pp. 1184–1194, Sep. 2004.

[3] F. Blaabjerg, R. Teodorescu, M. Liserre, and A. V. Timbus, "Overview of control and grid synchronization for distributed power generation systems," *IEEE Trans. Ind. Electron.*, vol. 53, no. 5, pp. 1398–1409, Oct. 2006.

[4] M. Dai, M. Marwali, J. Jung, and A. Keyhani, "Power flow control of a single distributed generation unit," *IEEE Trans. Power Electron.*, vol. 23, no. 1, pp. 343–352, Jan. 2008.

[5] R. H. Lasseter, "Microgrids," in *Proc. Power Eng. Soc. Winter Meeting*, Jan. 2002, vol. 1, pp. 305–308.

[6] N. Hatziargyriou, H. Asano, R. Iravani, and C. Marnay, "Microgrids," *IEEE Power Energy Mag.*, vol. 5, no. 4, pp. 78–94, Jul./Aug. 2007.

[7] J. A. P. Lopes, C. L. Moreira, and A. G. Madureira, "Defining control strategies for microgrids islanded operation," *IEEE Trans. Power Syst.*, vol. 21, no. 2, pp. 916–924, May 2006.

[8] A. Tuladhar, H. Jin, T. Unger, and K. Mauch, "Control of parallel inverters in distributed ac power systems with consideration of line impedance effect," *IEEE Trans. Ind. Appl.*, vol. 36, no. 1, pp. 131–138, Jan./Feb. 2000.

[9] M. C. Chandorkar and D. M. Divan, "Control of parallel connected inverters in standalone AC supply system," *IEEE Trans. Ind. Appl.*, vol. 29, no. 1, pp. 136–143, Jan./Feb. 1993.

[10] F. Katiraei and M. R. Iravani, "Power management strategies for a microgird with multiple distributed generation units," *IEEE Trans. Power Syst.*, vol. 21, no. 4, pp. 1821–1831, Nov. 2006.

[11] J. Guerrero, L. de Vicuna, J. Matas, M. Castilla, and J. Miret, "A wireless controller to enhance dynamic performance of parallel inverters in distributed generation system," *IEEE Trans. Power Electron.*, vol. 19, no. 5, pp. 1205–1213, Sep. 2004.

[12] S. J. Chiang, C. Y. Yen, and K. T. Chang, "A multimodule parallelable series-connected PWM voltage regulator," *IEEE Trans. Ind. Electron.*, vol. 48, no. 3, pp. 506–516, Jun. 2001.

[13] U. Borup, F. Blaabjerg, and P. Enjeti, "Sharing of nonlinear load in parallel-connected three-phase converters," *IEEE Trans. Ind. Appl.*, vol. 37, no. 6, pp. 1817–1823, Nov./Dec. 2001.

[14] T. Lin and P. Cheng, "Design of a new cooperative harmonic filtering strategy for distributed generation interface converters in an islanding network," *IEEE Trans. Power Electron.*, vol. 22, no. 5, pp. 1919–1927, Sep. 2007.

[15] R. C. Dugan, T. S. Key, and G. J. Ball, "Distributed resources standards," *IEEE Ind. Appl. Mag.*, vol. 12, no. 1, pp. 27–34, Jan.–Feb. 2006.

[16] Y.A.-R.I. Mohamed and E. F. El-Saadany, "Robust high-bandwidth discrete-time predictive current control with predictive internal model—A unified approach for voltage-source PWM converters," *IEEE Trans. Power Electron.*, vol. 23, no. 1, pp. 126–136, Jan. 2008.

[17] Y.A.-R.I. Mohamed and E. F. El-Saadany, "Hybrid variable-structure control with evolutionary optimum-tuning for fast grid-voltage regulation using inverter-based distributed generation," *IEEE Trans. Power Electron.*, vol. 23, no. 3, pp. 1334–1341, Jan. 2008.

[18] E. A. Coelho, P. C. Cortizo, and P. F. Carcia, "Small-signal stability of parallel-connected inverters in stand-alone AC supply systems," *IEEE Trans. Ind. Appl.*, vol. 38, no. 2, pp. 533–542, Mar.–Apr. 2002.

[19] Y. Makarov, Z. Dong, and D. Hill, "A general method for small signal stability analysis," *IEEE Trans. Power Syst.*, vol. 13, no. 3, pp. 979–985, Aug. 1998.

[20] C. Sao and P. Lehn, "Autonomous load sharing of voltage source converters," *IEEE Trans. Power Del.*, vol. 20, no. 2, pp. 1009–1016, Apr. 2005.

Yasser Abdel-Rady Ibrahim Mohamed was born in Cairo, Egypt, on November 25, 1977. He received the B.Sc. (with honors) and M.Sc. degrees in electrical engineering from Ain Shams University, Cairo, in 2000 and 2004, respectively, and the Ph.D. degree in electrical engineering from the University of Waterloo, Waterloo, ON, Canada, in 2008.

From 2002 to 2006, he was with the Aircraft Electric Network Laboratory, Aerospace Research Center, Cairo, as a Senior Research Engineer. From 2006 to 2008, he was a Research and Teaching Assistant in the Department of Electrical and Computer Engineering, University of Waterloo, where he is currently a Research Associate. His current research interests include distributed energy resources interfacing and control, high-performance motor drive systems for aerospace actuators, and robust and adaptive control theories and applications.

Dr. Mohamed is an Associate Editor of the IEEE TRANSACTIONS ON INDUSTRIAL ELECTRONICS. His biography is listed in the 2009 edition of Who's Who in the World.

Ehab F. El-Saadany (M'01–SM'05) was born in Cairo, Egypt, in 1964. He received the B.Sc. and M.Sc. degrees in electrical engineering from Ain Shams University, Cairo, Egypt, in 1986 and 1990, respectively, and the Ph.D. degree in electrical engineering from the University of Waterloo, Waterloo, ON, Canada, in 1998.

Currently, he is an Associate Professor in the Department of Electrical and Computer Engineering, University of Waterloo. His current research interests include distribution system control and operation, power quality, power electronics, digital signal processing applications to power systems, and mechatronics.